Journal of Systems Engineering and Electronics
Vol. 32, No. 6, December 2021, pp.1509 – 1526

Influence of roll-pitch seeker DRR and parasitic loop on Lyapunov stability of guidance system

LI Yue[1], WEN Xianghua[2,*], LI Wei[2], WEI Lan[2], and XIA Qunli[1]

1. School of Aerospace Engineering, Beijing Institute of Technology, Beijing 100081, China;
2. No. 5718 Factory, Chinese People's Liberation Army, Guilin 541002, China

Abstract: This paper focuses on the influence of the disturbance rejection rate (DRR) and parasitic loop parameters on the stability domain of the roll-pitch seeker's guidance system. The DRR models of the roll-pitch seeker caused by different types of disturbance torques and the scale deviation of different sensors are established. The optimal DRR model of the roll-pitch seeker, which contains the scale deviation model, is proposed by formula derivation. The model of the roll-pitch seeker's guidance system is established and equivalently simplified by the dimensionless method. The Lyapunov stability criterion for stability analysis of the guidance system is given by means of the passivity theorem and related definitions and lemmas. A simplified model of the roll-pitch seeker's guidance system, which is suitable for the Lyapunov stability criterion, is established by formula derivation and equivalent transformation. Three conditions that satisfy the Lyapunov stability criterion are obtained. Mathematical simulation with Nyquist plots is used to analyze the influence of different DRR parameters on the stability domain of the roll-pitch seeker's guidance system. Simulation results of this paper can provide reference for the stability analysis of systems related to the roll-pitch seeker.

Keywords: roll-pitch seeker, guidance system, disturbance rejection rate (DRR), parasitic loop, Lyapunov stability, Nyquist analysis.

DOI: 10.23919/JSEE.2021.000127

1. Introduction

Nowadays, the infrared air-to-air missile plays an important role in the air combat environment [1−4]. Improving the performance of the infrared air-to-air missile is important to obtain the superiority of air combat [5−7]. In today's world, the most advanced air-to-air missile is the fourth generation air-to-air missile, whose main innovation is to replace the traditional pitch-yaw seeker with the roll-pitch seeker. Compared with other air-to-air missiles equipped with the common pitch-yaw seeker, the air-to-air missiles equipped with the roll-pitch seeker have better application prospects in aspects of searching for targets and tracking maneuvering targets due to the roll-pitch seeker's advantages of a large field of view angle and a small volume [8,9]. Therefore, to improve the performance of the roll-pitch seeker becomes the key to improving performance of the infrared air-to-air missile in future air combat.

Due to the semi-strapdown structure, the line-of-sight (LOS) rate output by the roll-pitch seeker will be affected by the disturbance of the missile body [10−12]. The ratio of the roll-pitch seeker's LOS rate affected by the missile body disturbance to the missile body disturbance is defined as the disturbance rejection rate (DRR) of the roll-pitch seeker. In addition, the scale deviation among sensors of the roll-pitch seeker will also make the LOS rate inaccurate and affect the value of DRR [13−16]. The inaccurate LOS rate output caused by the DRR of the roll-pitch seeker will be continuously expanded through the guidance law, autopilot and other guidance system links. This positive feedback loop of the DRR based on the roll-pitch seeker guidance system is defined as the DRR parasitic loop of the roll-pitch seeker [17,18]. The existence of the DRR parasitic loop can seriously interfere with the stability of the guidance system of the roll-pitch seeker [19]. Therefore, we need to study the influence law of these parameters on the stability of the guidance system, which can be used to design the parameters of the guidance air-to-air missile in the next step.

Several researchers have studied the influence of the seeker DRR and the parasitic loop on the stability of the guidance system [20−24]. Li et al. [20] established the mathematical model of the seeker's DRR and the DRR parasitic loop, which are used to analyze the stability of the seeker. Liu et al. [21] established the mathematical

Manuscript received June 16, 2020.
*Corresponding author.
This work was supported by the Defense Science and Technology Key Laboratory Fund of Luoyang Electro-optical Equipment Institute, Aviation Industry Corporation of China (6142504200108).

model of the seeker guidance system and studied the effects of the seeker DRR and the parasitic loop on the guidance system. These studies [20,21] only established the relevant model of the seeker and qualitatively analyzed the influence of DRR and the parasitic loop on the stability of the guidance system, but did not use the appropriate criterion for quantitative analysis. Du et al. [22] studied the stability of the seeker guidance system based on the mathematical model and the Routh criterion. Liu et al. [23] analyzed the influence of the seeker DRR and the parasitic loop on the stability of the guidance system based on the Routh criterion, and further studied the influence of frame coupling on the guidance system. The Routh criterion is based on the "frozen time" assumption, and the "frozen time" assumption is not valid when the distance between the missile and the target is very short or the dynamics of the guidance system is very fast [25−27]. In this case, the Routh criterion will cause a large error when it is used to quantitatively analyze the influence of DRR and the parasitic loop on the stability of the guidance system. Therefore, these studies [22,23] should be further optimized. Chen et al. [24] used a new "Lyapunov stability criterion" to analyze the influence of seeker DRR and parasitic loop on the stability of the guidance system. This new criterion is based on the finite time stability theory of the time-varying system, which can avoid the large error of the final guidance stage caused by the Routh criterion [28,29]. However, this research [24] takes the platform seeker as the research object and the roll-pitch seeker is not involved.

At present, most of the researches on the roll-pitch seeker focus on the problem of angular velocity extraction and zenith pass [30−33], but there is lack of related researches on the stability of the guidance system. In order to fill the research gap in the stability analysis of the roll-pitch seeker's guidance system, this paper takes the roll-pitch seeker as the research object. The Lyapunov stability criterion is used to analyze the influence of DRR and parasitic loop parameters on the stability domain of the roll-pitch seeker's guidance system in this paper. First, a complete DRR model of the roll-pitch seeker is established, which not only considers the influence of different types of disturbance torque on DRR, but also considers the influence of different sensor scale deviations on DRR. The quantitative influence of scale deviation on DRR is derived by formulas, and the parasitic loop model of the roll-pitch seeker containing the DRR caused by scale deviation is established. Second, based on the application of the passivity theorem, related definitions and lemmas, the equivalent transformation model of the roll-pitch seeker's guidance system, which is suitable for the Lyapunov stability criterion, is established. By applying the Lyapunov stability criterion, three conditions for the guidance system to satisfy the stable state are obtained. Third, through mathematical simulation and analysis, the relationship between DRR and parasitic loop parameters of the roll-pitch seeker and the stability domain of the roll-pitch seeker's guidance system is obtained. The relationship between the stability of the guidance system and the corresponding parameters is simulated and analyzed. Under different conditions, schemes to improve the stability of the guidance system of the roll-pitch seeker are proposed.

The main contents of each section are as follows. Section 1 describes the stability problem of the roll-pitch seeker's guidance system, and lists several existing solutions. In Section 2, the complete DRR and parasitic loop models of the roll-pitch seeker are established, and the model of the guidance system is simplified by the dimensionless method. In Section 3, the guidance system model based on the Lyapunov stability criterion is established by applying the passivity theorem, and three conditions for the stability of the model are obtained. In Section 4, the relationship between different parameters and the stability domain of the guidance system is simulated and analyzed, and the scheme to improve the stability of the guidance system of the roll-pitch seeker is obtained. Section 5 summarizes the whole paper and gives conclusions and contribution of the research results.

2. Establishment of relevant models

2.1 Model of roll-pitch seeker's DRR

The roll-pitch seeker can track the target's motion and output LOS rate by moving the optical axis. Fig. 1 shows the optical axis of the roll-pitch seeker tracks the movement of the target in the longitudinal plane.

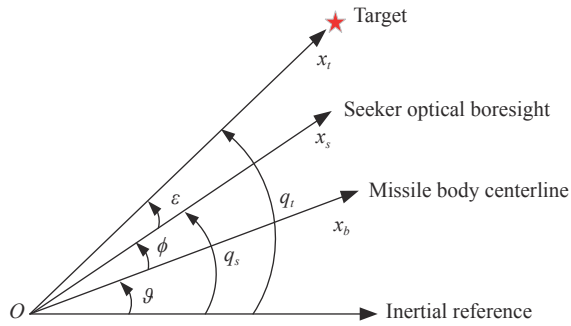

Fig. 1 Motion of roll-pitch seeker's optical axis

In Fig. 1, ϑ represents the pitch angle of the roll-pitch seeker. ϕ represents the frame angle of the roll-pitch seeker. q_t represents the real LOS angle, and q_s represents the optical axis angle of the roll-pitch seeker. Therefore, the detector error angle of roll-pitch seeker ε can be calculated as follows:

$$\varepsilon = q_t - q_s = q_t - \phi - \vartheta. \tag{1}$$

The detector error angle ε obtained by the motion of the roll-pitch seeker's optical axis can be transformed into the frame angular velocity instruction ω_{RC} of the roll-pitch seeker by sensor processing. The transfer process of instruction information is shown in Fig. 2.

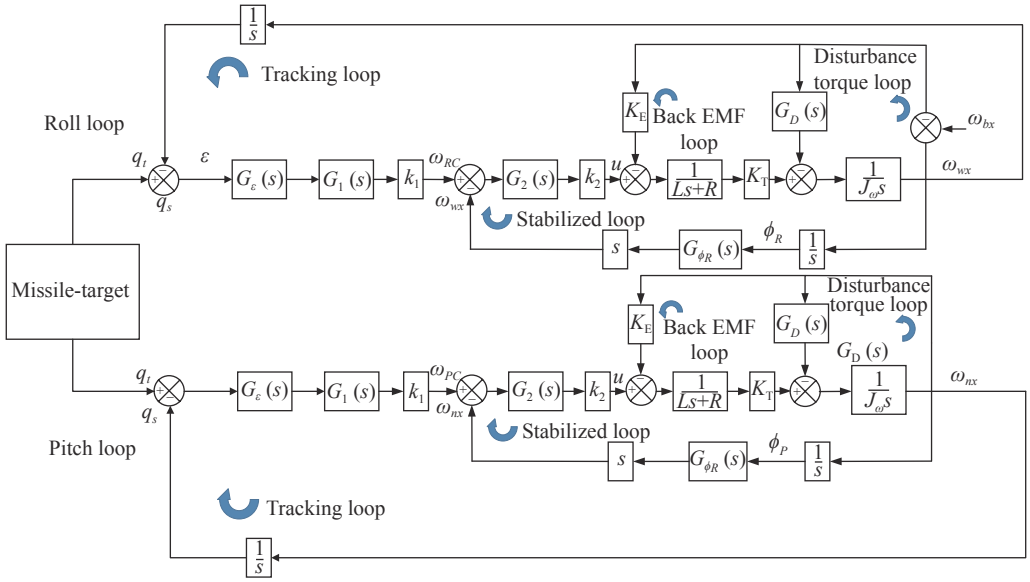

Fig. 2 Model of roll-pitch seeker's stabilized and tracking loops

In Fig. 2, the roll-pitch seeker model includes the outer loop (roll loop) and the inner loop (pitch loop). Both of the roll loop and the pitch loop have a tracking loop, a stabilized loop, a back eclipse modeling framework (EMF) loop, and a disturbance torque loop. The tracking loop is used to trace the target and output the LOS angle q_s. $G_\varepsilon(s)$, $G_1(s)$ and k_1 form the correction network of the tracking loop. The stabilized loop is used to stabilize the frame angular velocity and output the LOS rate ω_{wx} and ω_{nx}. $G_2(s)$ and k_2 form the correction network of the stabilized loop. L represents the motor inductance. R represents motor resistance. K_T represents torque constant. J_ω represents moment of inertia. $G_{\phi R}(s)$ and $G_{\phi P}(s)$ represent semi-strapdown calculation link. For the roll loop, in the case that the sensor scale deviation is not considered, the disturbance torque loop $G_D(s)$ and the back EMF loop K_E will couple missile body disturbance ω_{bx} to the frame angular rate calculation. For the pitch loop, in the case that the sensor scale deviation is not considered, the disturbance torque loop $G_D(s)$ and the back EMF loop K_E will couple missile body disturbance ω_{by}, ω_{bz} and roll frame angle ϕ_R to the frame angular rate calculation. Therefore, the existence of roll-pitch seeker's DRR is related to the disturbance torque loop and the back EMF loop.

Consider the case where only the disturbance torque loop $G_D(s)$ generates the DRR alone. There are two kinds of common disturbance torque for the roll-pitch seeker: spring torque and damping torque. Assume that K_n represents the spring torque coefficient, and K_ω represents the damping torque coefficient. Therefore, for both of the roll loop and the pitch loop, the disturbance torque loop parameter $G_D(s)$ can be represented as

$$G_D(s) = \frac{K_n}{s} + K_\omega. \tag{2}$$

The roll loop and the pitch loop are both coupled with the attitude disturbance of the missile body. The only difference of these two loops is that the pitch loop is also affected by the roll loop. As we can see from Fig. 2, for the roll loop, the missile body disturbance ω_{bx} is coupled to the stability loop, and the LOS rate ω_{wx} output by the stability loop is affected by the missile body disturbance ω_{bx}. For the pitch loop, the missile body disturbance ω_{by}, ω_{bz} and roll frame angle ϕ_R are coupled to the stability loop, and the LOS rate ω_{nx} output by the stability loop is affected by the missile body disturbance ω_{by}, ω_{bz} and roll frame angle ϕ_R. Therefore, the DRR of the roll loop and the pitch loop can be defined as

$$\begin{cases} R_{\text{roll}}(s) = \dfrac{\omega_{wx}}{\omega_{bx}} \times 100\% \\ R_{\text{pitch}}(s) = \dfrac{\omega_{nx}}{-\omega_{by}\sin\phi_R + \omega_{bz}\cos\phi_R} \times 100\% \end{cases}. \tag{3}$$

Although the two loops are affected by different

coupled disturbances, which means the inputs of disturbances are different. The factors causing the DRR are both the back EMF loop and the disturbance torque loop. According to Fig. 2 and (3), we find that the DRR transfer function (DRRTF) of the roll loop and the pitch loop is the same in the following form [30,32,33]:

$$R(s)=\frac{G_D(s)(Ls+R)+K_TK_E}{J_\omega Ls^2+(J_\omega R+G_D(s)L)s+G_2(s)K_T+K_TK_E}. \quad (4)$$

Consider the case that the disturbance torque is the spring torque or the damping torque separately, the DRRTF of the roll-pitch seeker will change into

$$R_n(s)=\frac{(K_nL+K_TK_E)s+K_nR}{J_\omega Ls^3+J_\omega Rs^2+(K_nL+K_TK_E+G_2(s)K_T)s}, \quad (5)$$

$$R_\omega(s)=\frac{K_\omega(Ls+R)+K_TK_E}{J_\omega Ls^2+(J_\omega R+K_\omega L)s+G_2(s)K_T+K_TK_E}. \quad (6)$$

We mainly study the causes of DRR and its influence on the stability of the guidance system. Since the DRRTF of both loops are the same in form, the research processes of the two loops are the same. For the convenience of the research, we only consider the roll loop of the roll-pitch seeker in the following research.

2.2 Influence of scale deviation on DRRTF

Due to the semi-strapdown structure, the roll-pitch seeker cannot directly output the LOS rate. The roll-pitch seeker requires two steps to obtain the LOS rate. Firstly, the LOS angle of the roll-pitch seeker should be reconstructed by the semi-strapdown calculation. Secondly, the LOS rate can be estimated by the kalman filter. In the semi-strapdown calculation, the detector sensor, the frame angle sensor and the angular rate sensor are used. The scale of these sensors is different, which will lead to inaccurate LOS angle by semi-strapdown calculation, and then lead to inaccurate estimation of the LOS rate. Therefore, the scale deviation will also cause the DRR problem for the roll-pitch seeker.

Assume that R_s represents the scale deviation between the detector and the angular rate sensor, R_m represents the scale deviation between the frame angle sensor and the angular rate sensor. Then, the DRR caused by the scale deviation of different sensors of the roll-pitch seeker, which is recorded as R_d, can be calculated as

$$R_d=\frac{\Delta\dot{q}}{\dot{\vartheta}}=(R_s+R_m)\times 100\%. \quad (7)$$

Since R_s and R_m vary within the range of 0.000 1 in a single flight, which can be ignored, R_d can be regarded as a fixed value in a single flight. Fig. 3 shows the optical axis motion of the roll-pitch seeker under the DRR effect caused by the scale deviation.

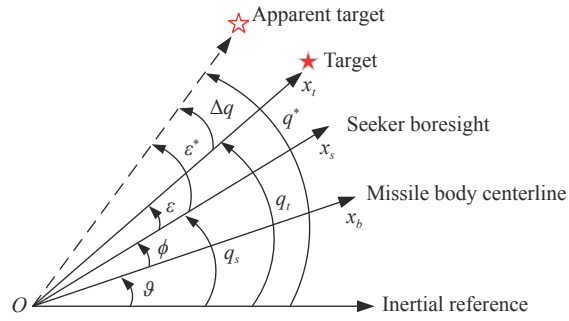

Fig. 3 Motion of roll-pitch seeker's optical axis affected by scale deviation

In Fig. 3, q^* represents the LOS angle detected by the roll-pitch seeker. ε^* represents the new detector error angle affected by R_d. Δq represents LOS angle deviation caused by R_d. R_d is the DRR caused by scale deviation among several kinds of sensors in the semi-strawdown calculation. Since the input and output of the semi-strapdown calculation of the roll-pitch seeker are quantities that are related to frame angle ϕ, the relationship between the LOS angle deviation Δq and R_d can be assumed as

$$\Delta q=R_d\phi. \quad (8)$$

According to the geometric relationship in Fig. 3, (8) can be transformed into

$$q^*=q_t+(q_s-\vartheta)R_d. \quad (9)$$

Assuming that the tracking process of the roll-pitch seeker to the target is stable, the detector error angle ε can be regarded as a small quantity, which means that

$$q_s\cong q_t. \quad (10)$$

From (10), (9) can be transformed into

$$q^*\cong q_t+(q_t-\vartheta)R_d=q_t(1+R_d)-\vartheta R_d. \quad (11)$$

Generally speaking, R_d is far less than 1, so (11) can be transformed into

$$q^*=q_t-\vartheta R_d. \quad (12)$$

Equation (12) shows the relationship between the LOS angle, the attitude angle and the DRR. Considering the DRR caused by the scale deviation, Fig. 2 can be modified into Fig. 4.

According to [21,24,27] and typical experimental data, the range of k_2 is generally 10 to 100, the range of K_E is generally 0 to 0.01, and the range of $G_D(s)$ is generally 0 to 0.01. Therefore, we can obtain that $K_EK_T\ll k_2K_T$, and $G_D(s)/J_\omega\ll k_2K_T/J_\omega$. The back EMF loop and $G_D(s)/J_\omega$ can be ignored. Fig. 4 will be simplified into Fig. 5.

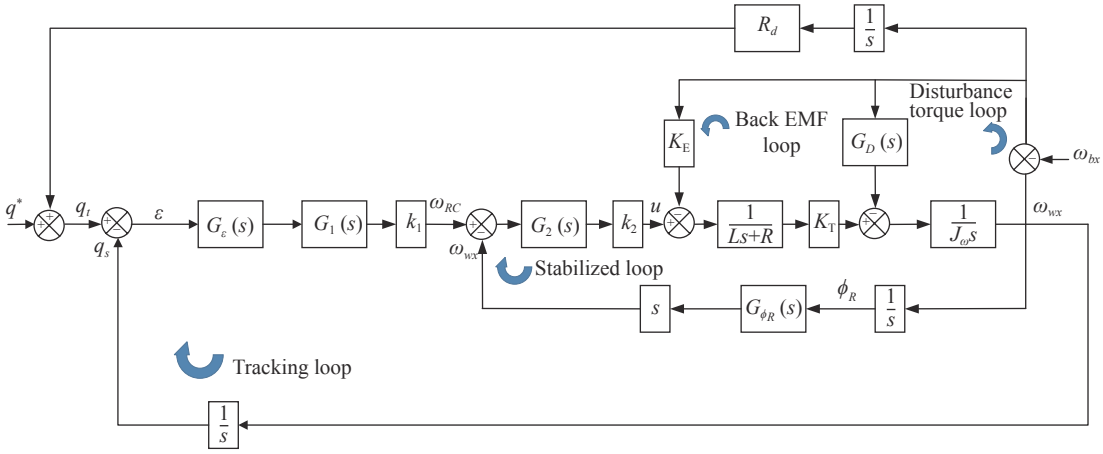

Fig. 4 Model of roll-pitch seeker affected by DRR

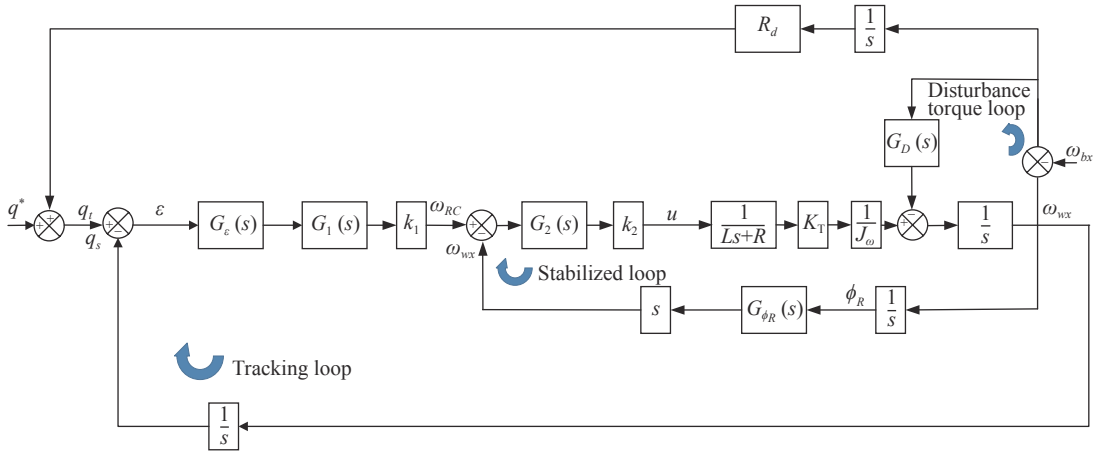

Fig. 5 Simplified model of roll-pitch seeker with disturbances

In the stabilized loop of the roll-pitch seeker system, ω_{wx} represents the angular rate of the frame. Since angular rate gyro is not installed on the frame of the roll-pitch seeker, ω_{wx} cannot be measured directly. We should firstly calculate the frame angle ϕ_R by measured quantity, and then extract the frame angular rate ω_{wx} by a differentiator. This process is called the semi-strapdown calculation of the roll-pitch seeker. $G_{\phi R}(s)$ represents the calculation error gain of frame angle ϕ_R. In the ideal state, the calculation error of frame angle ϕ_R is very small, and error gain $G_{\phi R}(s) \approx 1$. The input and output of the whole semi-strpdown calculation process are the frame angular rate ω_{wx}. For the convenience of subsequent research, the system can be further simplified into Fig. 6.

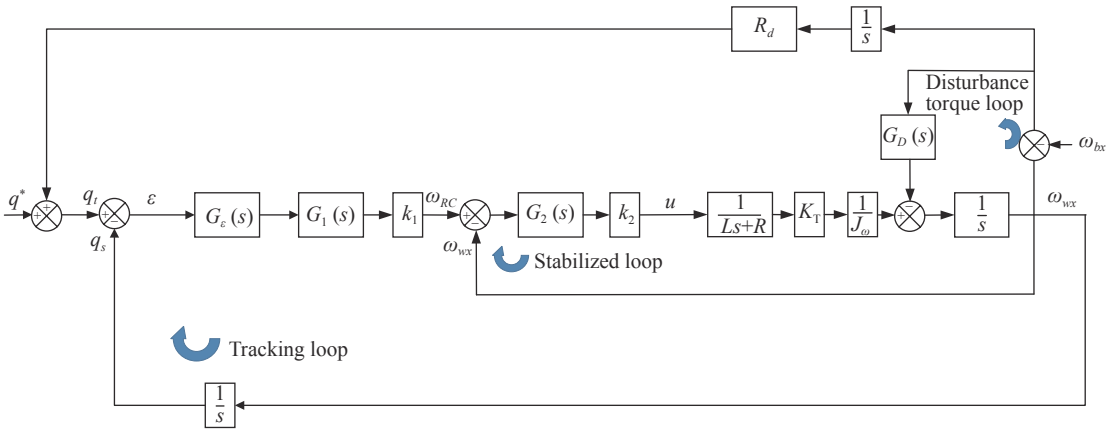

Fig. 6 Simplified model of roll-pitch seeker without semi-strapdown calculation

For further analysis, the roll-pitch seeker model shown in Fig. 6 can be simplified. According to common practices [18,21,30,31] of seeker loop DRR research, we can assume that $L \cong 0, R \cong 1$[18,31,32,33], and ignore the influence of the back EMF loop with the reason of $K_E K_T \ll k_2 K_T$ and ignore the details of semi-strawdown calculation. Equivalent gain of the tracking loop is recorded as K_1, and the equivalent gain of the stabilized loop is recorded as K_2. From Fig. 6, we can obtain that

$$K_1 = k_1 G_\varepsilon G_1, \tag{13}$$

$$K_2 = k_2 K_T G_2 / J_\omega. \tag{14}$$

Therefore, Fig. 6 can be simplified into Fig. 7.

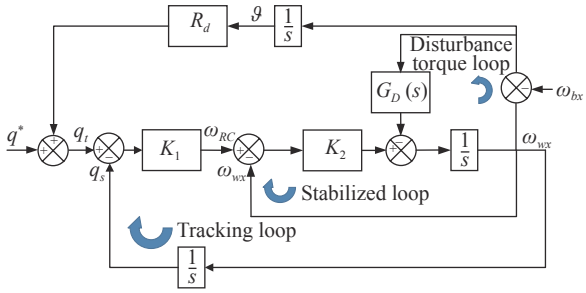

Fig. 7 Simplified model of roll-pitch seeker affected by DRR

From Fig. 7, we can obtain the modified DRRTF with $K_r = R_d/(1-R_d)$:

$$R(s) = \frac{\Delta\dot{q}(s)}{\dot{\vartheta}(s)} = \frac{-K_r + sG_D(s)/K_1K_2}{(1/K_1K_2)s^2 + ((G_D(s)+K_2)/K_1K_2)s + 1}. \tag{15}$$

Compared with (4), (15) increases the DRR caused by the scale deviation. Because $K_1K_2 \gg K_n$ and K_ω, based on the basic requirements of the seeker control system, time delay process, correction network and high frequency dynamics can be ignored for convenient analysis. Under the combined action of disturbance torque and scale deviation, the DRRTF $R(s)$ can be simplified into a first-order model, which is shown in Table 1. T_s is an equivalent time constant.

Table 1 Simplified first-order model of roll-pitch seeker's DRRTF

Disturbance torque	DRRTF	Equivalent coefficient
Spring torque	$R_n(s) = \frac{K_s - K_r}{T_s s + 1}$	$K_s = \frac{K_n}{K_1 K_2}$
Damping torque	$R_\omega(s) = \frac{sK_v - K_r}{T_s s + 1}$	$K_v = \frac{K_\omega}{K_1 K_2}$

2.3 Model of guidance system

The inaccurate LOS rate caused by the scale deviation will generate the wrong control instructions through the guidance law and autopilot, and then generate additional attitude movement of the missile body. This kind of vicious circle is defined as the DRR parasitic loop. Fig. 8 shows the model of the roll-pitch seeker guidance system with a DRR parasitic loop.

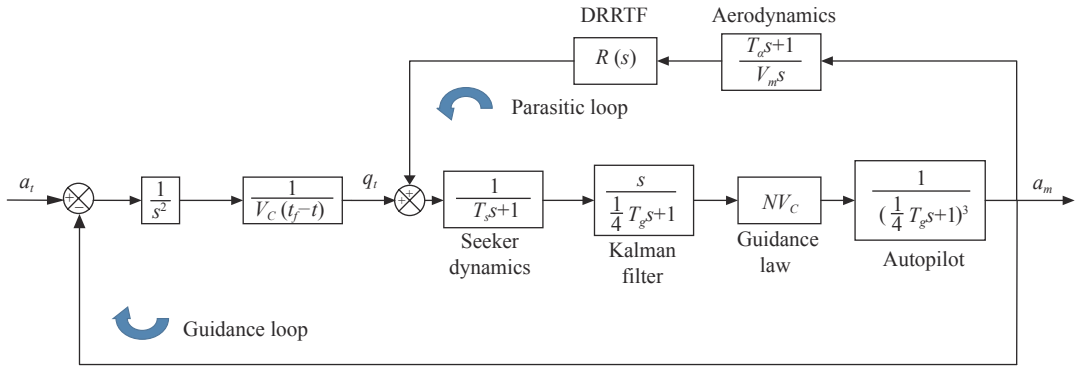

Fig. 8 Guidance system model of roll-pitch seeker with parasitic loop

In Fig. 8, N is the proportional guidance coefficient, the input of the guidance loop is the target maneuvering acceleration, and the output is the missile acceleration. V_c represents the relative speed of the missile and the target. $t_{go} = t_f - t$ represents remaining flight time. T_s represents equivalent time constant. T_g represents guidance time constant. T_α represents angle of attack time constant. $R(s)$ represents the DRR under the combined action of the disturbance torque and scale deviation. Simplified models of seeker dynamics, filters, guidance laws, and autopilot are all shown in Fig. 8.

Conduct the following dimensionless operation on each link of the guidance system as shown in Fig. 8:

$$\begin{cases} \bar{s} = T_g s \\ \bar{t}_f = t_f / T_g \\ \bar{T}_\alpha = T_\alpha / T_g \\ \bar{T}_s = T_s / T_g \end{cases}. \tag{16}$$

The roll-pitch seeker guidance system with a parasitic loop shown in Fig. 8 can be simplified to the dimensionless guidance system model in Fig. 9.

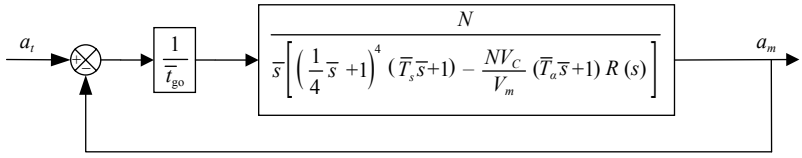

Fig. 9 Dimensionless guidance system model

3. Lyapunov stability criterion of roll-pitch seeker's guidance system

3.1 Definition of Lyapunov stability

Based on the analysis of Section 2, we obtain the dimensionless simplified model of the roll-pitch seeker's guidance system with the DRR parasitic loop. Analyzing the influence of different parameters on the stability of the guidance system is the key to the next step. Since the guidance system shown in Fig. 9 is a time-varying system, the Nyquist criterion and the Routh criterion, which are commonly used to analyze the stability of time-invariant systems, are no longer applicable. The Lyapunov stability criterion is used to analyze the stability of linear time-varying systems and nonlinear systems. Therefore, it is appropriate to select the Lyapunov stability criterion to analyze the stability of the roll-pitch seeker's guidance system.

Definition 1 Stability in the sense of Lyapunov

If $\dot{x}=f(t,x)$ is a time-varying system, and $\dot{x}(0)=f(t,0)=0,\forall t\geqslant 0$, then, $x=0$ is defined as the equilibrium point of the system. This equilibrium point is (i) uniformly stable in the sense of Lyapunov if each $\xi>0$ has $\delta=\delta(\xi)>0$ independent of t_0 such that $\|x(t_0)\|<\delta\Rightarrow\|x(t)\|<\xi,\forall t\geqslant t_0\geqslant 0$, and (ii) uniformly asymptotically stable in the sense of Lyapunov if it is uniformly stable and has a positive constant c independent of t_0, for each $\eta>0, T=T(\eta)>0$ is observed, such that $\|x(t)\|<\eta$, $\forall t\geqslant t_0+T(\eta),\forall\|x(t_0)\|<c$.

A time-varying system, which is uniformly stable or uniformly asymptotically stable in the sense of Lyapunov, can be considered stable in the sense of Lyapunov. For the guidance system of the roll-pitch seeker, a uniformly stable time-varying system cannot guarantee the stability in practical application, and only a uniformly asymptotically stable system can meet the requirements of practical application. Therefore, we need to use the Lyapunov stability criterion to analyze the range variation of the uniform asymptotic stability domain of the roll-pitch seeker's guidance system under the influence of different parameters.

3.2 Lyapunov stability criterion represented by passivity theorems

Usually, the method of using the Lyapunov stability criterion is to construct the Lyapunov function of the time-varying system, and judge the stability of the system by the judge properties of the function. However, it is very difficult to directly construct the Lyapunov function of the roll-pitch seeker's guidance system in Fig. 9. Therefore, we use another indirect method, which requires the use of the passivity theorem, to apply the Lyapunov stability criterion. Some relevant definitions and lemmas of the passivity theorem are given as follows.

Definition 2 Passivity of time-varying memoryless systems

The system $y=h(t,u)$ is defined as a time-varying memoryless system if the output of the system is independent of state variables. If h satisfies the inequality: $\alpha u^2\leqslant uh(t,u)\leqslant\beta u^2$ for all (t,u), where α and β are real numbers with $\beta\geqslant\alpha$, then h belongs to the sector $[\alpha,\beta]$. If h belongs to the sector $[0,\infty]$, then the system $y=h(t,u)$ is defined as passive. If h belongs to the sector $(0,\infty)$, then the system $y=h(t,u)$ is defined as strictly passive.

Definition 3 Strictly positive real transfer function

The single-input-single-output linear system transfer function $G(s)$ is defined as the strictly positive real function if and only if: (i) $G(\infty)>0$, (ii) all poles of $G(s)$ are in $\mathrm{Re}[s]<0$, and (iii) $\mathrm{Re}[G(j\omega)]>0,\forall\omega>0$.

Lemma 1 Relationship between positive real and passivity properties[34]

The system $\dot{x}=\boldsymbol{A}x+\boldsymbol{B}u$, $y=\boldsymbol{C}x+\boldsymbol{D}u$ is a linear time invariant system. If the transfer function $G(s)=\boldsymbol{C}(s\boldsymbol{I}-\boldsymbol{A})^{-1}\boldsymbol{B}+\boldsymbol{D}$ is strictly positive real, then the linear time invariant system is the strictly passive system. $\boldsymbol{A}$, $\boldsymbol{B}$, $\boldsymbol{C}$, $\boldsymbol{D}$ are constant matrices, and $\boldsymbol{I}$ is the unit matrix.

Lemma 2 Lyapunov stability criterion represented by passivity theorems[35]

Consider the feedback connection of a strictly passive, time-invariant system $Y(s)$ with a passive, time varying, memoryless function $h(t,u)$, which is shown in Fig. 10.

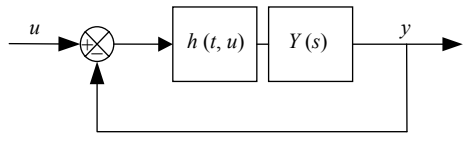

Fig. 10 Feedback connection

Then, the origin of the closed loop system shown in Fig. 10 is uniformly asymptotic stability in the sense of Lyapunov.

3.3 Loop transformation for application of Lyapunov stability criterion

Comparing the roll-pitch seeker's guidance system in Fig. 9 with the feedback-connected closed-loop system in Fig. 10, we know that the Lyapunov stability of the roll-pitch seeker's guidance system can be analyzed by Lemma 2. The functions in Fig. 9 can be expressed as $h(t,u)$ and $Y(s)$:

$$h(t,u)=\frac{1}{\bar{t}_{go}}=\frac{1}{\bar{t}_f-\bar{t}}, \tag{17}$$

$$Y(s)=\frac{N}{\bar{s}\left[\left(\frac{1}{4}\bar{s}+1\right)^4\left(\bar{T}_s\bar{s}+1\right)-\frac{NV_C}{V_m}\left(\bar{T}_\alpha\bar{s}+1\right)R(s)\right]}. \tag{18}$$

However, $h(t,u)$ and $Y(s)$ in Fig. 9 do not satisfy the conditions in Lemma 2. In order to apply Lemma 2 for stability analysis of the roll-pitch seeker's guidance system, $h(t,u)$ and $Y(s)$ in Fig. 9 need to be transformed into equivalent systems that satisfy the conditions in Lemma 2. If $h(t,u)$ is a time varying, memoryless function, which belongs to the sector $[\alpha,\beta]$, and $Y(s)$ is a time-invariant system, then $h(t,u)$ and $Y(s)$ can be transformed into Fig. 11.

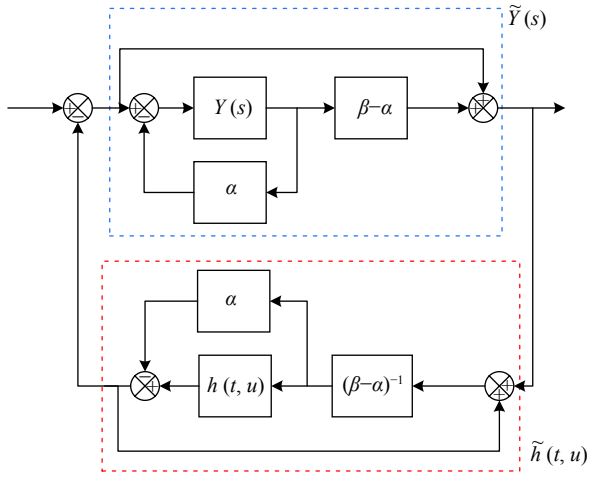

Fig. 11 Equivalent feedback connection

Systems shown in Fig. 9 and Fig. 11 are equivalent in terms of stability. In Fig. 11, $h(t,u)$ and $Y(s)$ are all transformed into equivalent feedback connection $\tilde{h}(t,u)$ and $\tilde{Y}(s)$. $h(t,u)$ belongs to the sector $[\alpha,\beta]$ in Fig. 10, and $\tilde{h}(t,u)$ belongs to $[0,\infty]$ in Fig. 11. $\tilde{h}(t,u)$ in Fig. 11 is a passive, time varying, memoryless function. According to Lemma 2, if $\tilde{Y}(s)$ is a strictly passive, time-invariant system, the origin of closed loop system shown in Fig. 11 is uniformly asymptotic stability in the sense of Lyapunov. According to Lemma 1, if the constructed function $G(s)=\boldsymbol{C}(s\boldsymbol{I}-\boldsymbol{A})^{-1}\boldsymbol{B}+\boldsymbol{D}$ of the time-invariant system $\tilde{Y}(s)$ is strictly positive real, then the time-invariant system $\tilde{Y}(s)$ is the strictly passive system and the origin of the closed loop system shown in Fig. 11 is uniformly asymptotic stability in the sense of Lyapunov.

$\bar{t}_k$ represents any moment of the terminal guidance, and the stability of the guidance system within a certain time frame $\bar{t}\in[0,\bar{t}_k]$ is discussed. From (17), we know that

$$h(t,u)\in\left[\frac{1}{\bar{t}_f},\frac{1}{(\bar{t}_f-\bar{t}_k)}\right]. \tag{19}$$

The sector of $h(t,u)$ can be expressed as $[\alpha,\beta]$, which means

$$\alpha=\frac{1}{\bar{t}_f}, \tag{20}$$

$$\beta=\frac{1}{(\bar{t}_f-\bar{t}_k)}. \tag{21}$$

$h(t,u)$ in (19) is not passive, so $h(t,u)$ needs to be transformed into $\tilde{h}(t,u)$, which belongs to $[0,\infty]$. The transformation process is shown in Fig. 11, and $Y(s)$ needs to be transformed into $\tilde{Y}(s)$, too. Then, we can obtain the constructed function:

$$\tilde{G}(\bar{s})=\frac{\bar{s}\left[\left(\frac{\bar{s}}{4}+1\right)^4\left(\bar{T}_s\bar{s}+1\right)-N\frac{V_C}{V_m}R(s)\left(\bar{T}_\alpha\bar{s}+1\right)\right]+\frac{N}{\bar{t}_f-\bar{t}_k}}{\bar{s}\left[\left(\frac{\bar{s}}{4}+1\right)^4\left(\bar{T}_s\bar{s}+1\right)-N\frac{V_C}{V_m}R(s)\left(\bar{T}_\alpha\bar{s}+1\right)\right]+\frac{N}{\bar{t}_f}}. \tag{22}$$

According to the above analysis, we draw a conclusion that if $\tilde{G}(s)$ in (22) is strictly positive real, systems in Fig. 11 and Fig. 9 are uniformly asymptotic stability in the sense of Lyapunov within a certain time frame $\bar{t}\in[0,\bar{t}_k]$. From Definition 3, we know that there are three conditions for $\tilde{G}(s)$ to be strictly positive real:

(i) By substituting DRRTF in Table 1 into (22), for the spring torque,

$$\tilde{G}(\bar{s})=\frac{\bar{s}\left[\left(\frac{\bar{s}}{4}+1\right)^4\left(\bar{T}_s\bar{s}+1\right)-N\frac{V_C}{V_m}(K_s-K_r)\frac{\left(\bar{T}_\alpha\bar{s}+1\right)}{\left(\bar{T}_s\bar{s}+1\right)}\right]+\frac{N}{\bar{t}_f-\bar{t}_k}}{\bar{s}\left[\left(\frac{\bar{s}}{4}+1\right)^4\left(\bar{T}_s\bar{s}+1\right)-N\frac{V_C}{V_m}(K_s-K_r)\frac{\left(\bar{T}_\alpha\bar{s}+1\right)}{\left(\bar{T}_s\bar{s}+1\right)}\right]+\frac{N}{\bar{t}_f}} \tag{23}$$

where $\bar{T}_s$, N, V_C, V_m, K_s, K_r, $\bar{T}_\alpha$, $\bar{t}_f$, $\bar{t}_k$ are constants. According to the limit calculation rule and L'Hopital's rule:

$$\begin{cases} \tilde{A}=\lim\limits_{\bar{s}\to\infty}\left[N\dfrac{V_C}{V_m}(K_s-K_r)\dfrac{\left(\bar{T}_\alpha\bar{s}+1\right)}{\left(\bar{T}_s\bar{s}+1\right)}\right]=N\dfrac{V_C}{V_m}(K_s-K_r)\dfrac{\bar{T}_\alpha}{\bar{T}_s} \\ \tilde{B}=\lim\limits_{\bar{s}\to\infty}\left[\left(\dfrac{\bar{s}}{4}+1\right)^4\left(\bar{T}_s\bar{s}+1\right)\right]=\infty \\ \tilde{C}=\lim\limits_{\bar{s}\to\infty}\dfrac{N}{\bar{t}_f-\bar{t}_k}=\dfrac{N}{\bar{t}_f-\bar{t}_k} \\ \tilde{D}=\lim\limits_{\bar{s}\to\infty}\dfrac{N}{\bar{t}_f}=\dfrac{N}{\bar{t}_f} \end{cases}. \tag{24}$$

Since $\tilde{A}$, $\tilde{C}$, $\tilde{D}$ are constants, according to the limit calculation rule and L'Hopital's rule, from (24), we can obtain

$$\lim_{\bar{s}\to\infty}\tilde{G}(\bar{s})=\lim_{\bar{s}\to\infty}\frac{\bar{s}\left[\tilde{B}-\tilde{A}\right]+\tilde{C}}{\bar{s}\left[\tilde{B}-\tilde{A}\right]+\tilde{D}}=1. \tag{25}$$

For the damping torque,

$$\tilde{G}(\bar{s})=\frac{\bar{s}\left[\left(\dfrac{\bar{s}}{4}+1\right)^4\left(\bar{T}_s\bar{s}+1\right)-N\dfrac{V_C}{V_m}(sK_v-K_r)\dfrac{\left(\bar{T}_\alpha\bar{s}+1\right)}{\left(\bar{T}_s\bar{s}+1\right)}\right]+\dfrac{N}{\bar{t}_f-\bar{t}_k}}{\bar{s}\left[\left(\dfrac{\bar{s}}{4}+1\right)^4\left(\bar{T}_s\bar{s}+1\right)-N\dfrac{V_C}{V_m}(sK_v-K_r)\dfrac{\left(\bar{T}_\alpha\bar{s}+1\right)}{\left(\bar{T}_s\bar{s}+1\right)}\right]+\dfrac{N}{\bar{t}_f}} \tag{26}$$

where $\bar{T}_s, N, V_C, V_m, K_v, K_r, \bar{T}_\alpha, \bar{t}_f, \bar{t}_k$ are constants. According to the limit calculation rule and L'Hopital's rule, in (26), we can obtain that

$$\begin{aligned}\tilde{A}=\lim_{\bar{s}\to\infty}\left[\left(\frac{\bar{s}}{4}+1\right)^4\left(\bar{T}_s\bar{s}+1\right)-N\frac{V_C}{V_m}(sK_v-K_r)\frac{\left(\bar{T}_\alpha\bar{s}+1\right)}{\left(\bar{T}_s\bar{s}+1\right)}\right]=\lim_{\bar{s}\to\infty}\left[\left(\frac{\bar{s}}{4}+1\right)^4\left(\bar{T}_s\bar{s}+1\right)\right]-N\frac{V_C}{V_m}\frac{\bar{T}_\alpha}{\bar{T}_s}\lim_{\bar{s}\to\infty}(sK_v-K_r)= \\ \lim_{\bar{s}\to\infty}\left[\left(\frac{\bar{s}}{4}+1\right)^4\frac{\left(\bar{T}_s\bar{s}+1\right)}{(sK_v-K_r)}\right]-N\frac{V_C}{V_m}\frac{\bar{T}_\alpha}{\bar{T}_s}=\frac{\bar{T}_s}{K_v}\lim_{\bar{s}\to\infty}\left[\left(\frac{\bar{s}}{4}+1\right)^4\right]-N\frac{V_C}{V_m}\frac{\bar{T}_\alpha}{\bar{T}_s}=\infty,\end{aligned} \tag{27}$$

$$\tilde{C}=\lim_{\bar{s}\to\infty}\frac{N}{\bar{t}_f-\bar{t}_k}=\frac{N}{\bar{t}_f-\bar{t}_k}, \tag{28}$$

$$\tilde{D}=\lim_{\bar{s}\to\infty}\frac{N}{\bar{t}_f}=\frac{N}{\bar{t}_f}. \tag{29}$$

Since $\tilde{C}$ and $\tilde{D}$ are constants, according to the limit calculation rule and the L'Hopital's rule, from (26), (27), (28), and (29) we can obtain

$$\lim_{\bar{s}\to\infty}\tilde{G}(\bar{s})=\lim_{\bar{s}\to\infty}\frac{\bar{s}\tilde{A}+\tilde{C}}{\bar{s}\tilde{A}+\tilde{D}}=1. \tag{30}$$

From (25) and (30), we find that $\tilde{G}(\infty)=1>0$ for both the spring torque and the damping torque. Therefore, the first condition is satisfied.

(ii) By using the Routh criterion to analyze the poles' distribution of $\tilde{G}(s)$, substitute DRRTF in Table 1 into the characteristic equation, the expansion characteristic equations for the spring torque and the damping torque are

$$\begin{aligned}\Phi_n(G(s))=\frac{1}{25\,600}\bar{s}^6+\frac{29}{6\,400}\bar{s}^5+\frac{53}{800}\bar{s}^4+\left[\frac{77}{200}+\frac{6}{100}\bar{T}_\alpha(K_r-K_s)\right]\bar{s}^3+ \\ \left[\frac{101}{100}+\frac{6}{100}(K_r-K_s)+6\bar{T}_\alpha(K_r-K_s)\right]\bar{s}^2+\left[1+6(K_r-K_s)\right]\bar{s}+\frac{4}{\bar{t}_f},\end{aligned} \tag{31}$$

$$\begin{aligned}\Phi_\omega(G(s))=\frac{1}{25\,600}\bar{s}^6+\frac{29}{6\,400}\bar{s}^5+\left(\frac{53}{800}-\frac{6}{100}K_v\bar{T}_\alpha\right)\bar{s}^4+\left[1+6K_r\right]\bar{s}+\frac{4}{\bar{t}_f}+ \\ \left[\frac{77}{200}-\frac{6}{100}K_v+\frac{6}{100}\bar{T}_\alpha K_r-6K_v\bar{T}_\alpha\right]\bar{s}^3+\left[\frac{101}{100}-6K_v+\frac{6}{100}K_r+6\bar{T}_\alpha K_r\right]\bar{s}^2.\end{aligned} \tag{32}$$

Table 2 gives the selection ranges of parameters. $\bar{t}_f$ is the dimensionless terminal guidance time, which cannot be too short for precision attack. According to the calculation method of Rouse criterion coefficients and the parameters selection range in Table 2, we can calculate the coefficients one by one. We can draw conclusions that the coefficients in the first column of the Rouse criterion coefficient list are almost all greater than zero, which means that all poles of $\tilde{G}(s)$ are distributed in the open left-half complex plane. Therefore, the second condition is satisfied.

(iii) The third condition requires that the Nyquist plots

of $\tilde{G}(\mathrm{j}\bar{\omega})$ are distributed in the right-half complex plane for each $\bar{\omega}$. Therefore, the distribution of Nyquist plots of $\tilde{G}(\mathrm{j}\bar{\omega})$ under the influence of different parameters need to be analyzed in the next section.

Table 2 Parameters that affect the stability of the guidance system

Parameter	Physical meaning	Parameter type	Values range
$\bar{T}_s$	Dimensionless equivalent time constant	Constant	0.01
N	Proportional guidance coefficient	Constant	4
V_c/V_m	The ratio of relative velocity to missile velocity	Constant	1.5
$\bar{T}_\alpha$	Dimensionless angle of attack time constant	Variable	1−3
$\bar{t}_f$/s	Dimensionless terminal guidance time	Variable	6−15
K_s	Spring torque equivalent coefficient	Variable	0−0.01
K_v	Damping torque equivalent coefficient	Variable	0−0.01
K_r	DRR equivalent coefficient	Variable	−0.03−0.03

4. Simulations and analysis

From the analysis in the previous chapter, we can draw the conclusion that if the Nyquist plots of $\tilde{G}(\mathrm{j}\bar{\omega})$ in (22) are distributed in the right-half complex plane for each $\bar{\omega}$, and then systems in Fig. 9 and Fig. 11 are uniformly asymptotic stability in the sense of Lyapunov within a certain time frame $\bar{t}\in[0,\bar{t}_k]$. From (22), we know that several parameters may affect the distribution of Nyquist plots. These parameters and their physical meanings and values are listed in Table 2.

All the parameters listed in Table 2 will affect the Nyquist plot distribution of $\tilde{G}(\mathrm{j}\bar{\omega})$ and thus affect the range of the stability domain of the roll-pitch seeker's guidance system. We focus on the analysis of the influence of $\bar{T}_\alpha,\bar{t}_f,K_s,K_v,K_r$ on the range of the stability domain of the roll-pitch seeker's guidance system. Fig. 12 shows the Nyquist plots of critical stable states with different K_r under spring torques. Fig. 13 shows the Nyquist plots of critical stable states with different K_r under damping torques. Fig. 14 shows the Nyquist plots of critical stable states with different K_r and invariant t_k under spring torques. Fig. 15 shows the Nyquist plots of critical stable states with different K_r and invariant t_k under damping torques. From Fig. 12 to Fig. 15, we know that under the action of the spring torque or the damping torque, when K_r is negative, $\bar{t}_k$ that makes the roll-pitch seeker's guidance system reach the stable state is larger than that when K_r is positive. This indicates that when other conditions are the same, the roll-pitch seeker's guidance system is more likely to be in a stable state if K_r is negative.

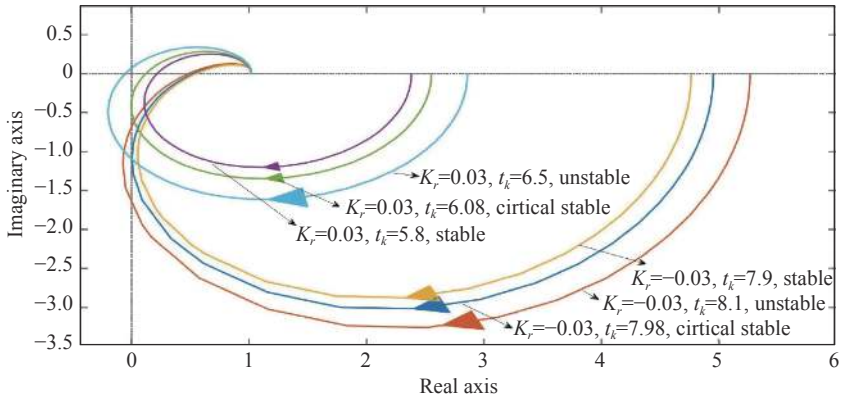

Fig. 12 Nyquist plot of different K_r with spring torque

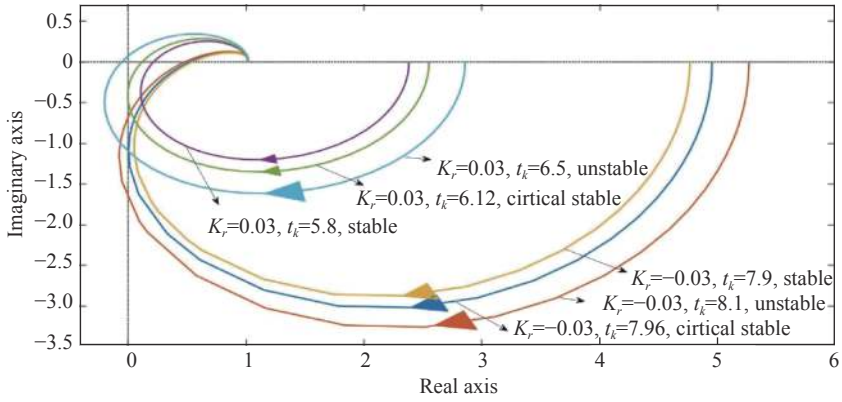

Fig. 13 Nyquist plot of different K_r with damping torque

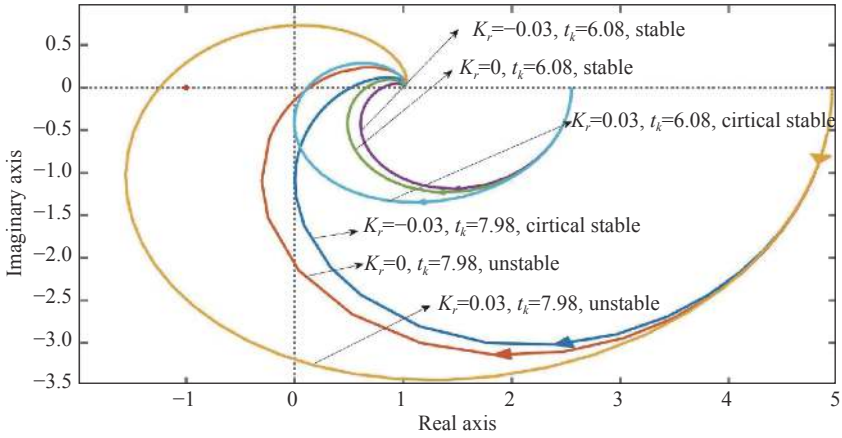

Fig. 14 Nyquist plot of invariant t_k with spring torque

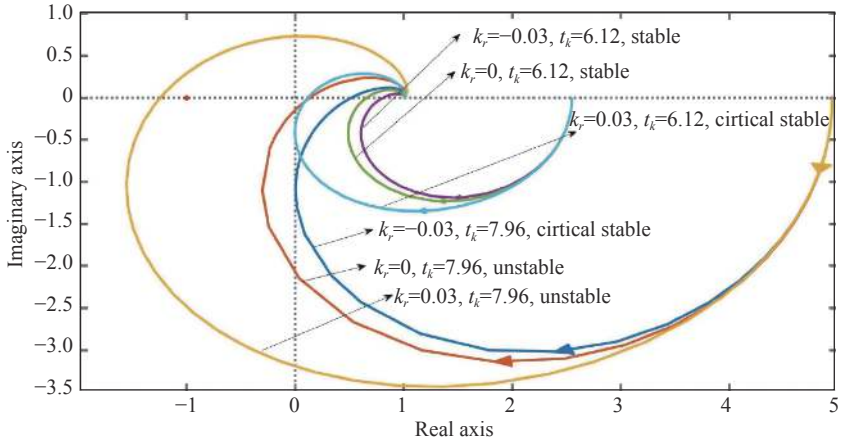

Fig. 15 Nyquist plot of invariant t_k with spring torque

Under the condition that the final guidance time $\bar{t}_f$ is 7 s, 10 s and 15 s respectively, the relationship between the unstable state time interval of the roll-pitch seeker's guidance system and the spring torque coefficient or damping torque coefficient is considered in Figs. 16−19. $\bar{t}_{\text{uns}} = \bar{t}_f - \bar{t}_k$ represents the time interval of the unstable state. Within the same terminal guidance time, the larger the time interval of the unstable state $\bar{t}_{\text{uns}}$ is, the shorter the time interval of the stable state of the guidance system is, and the more severe the condition that satisfies the stable state requirements of the guidance system will be. Fig. 16 and Fig. 17 show the relationship between the time interval of

unstable state $\bar{t}_{\text{uns}}$ and spring torque coefficient K_s with different K_r. Fig. 18 and Fig. 19 show the relationship between unstable state time interval $\bar{t}_{\text{uns}}$ and damping torque coefficient K_v with different K_r.

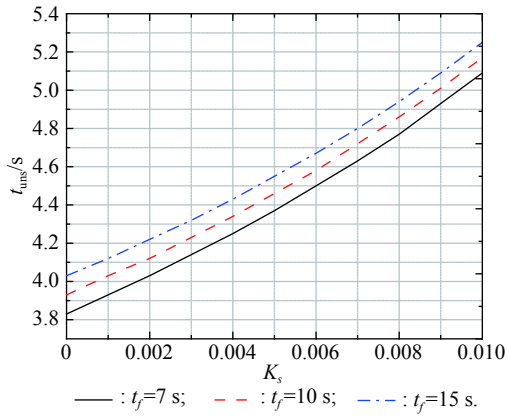

Fig. 16 Relationship between the unstable interval and K_s (K_r=0.03)

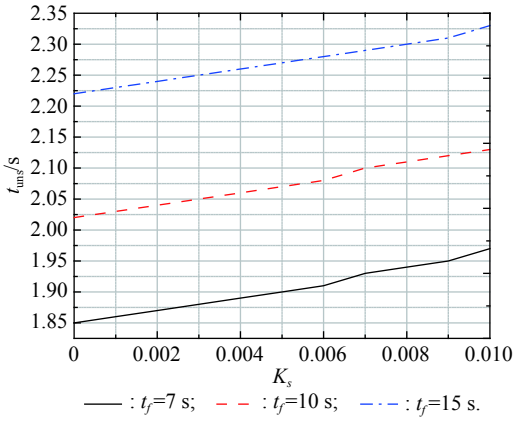

Fig. 17 Relationship between the unstable interval and K_s (K_r=−0.03)

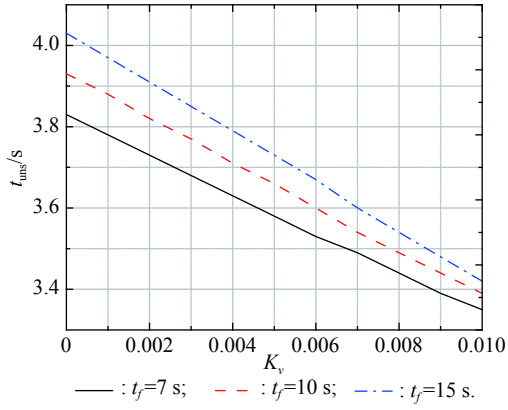

Fig. 18 Relationship between the unstable interval and K_v (K_r=0.03)

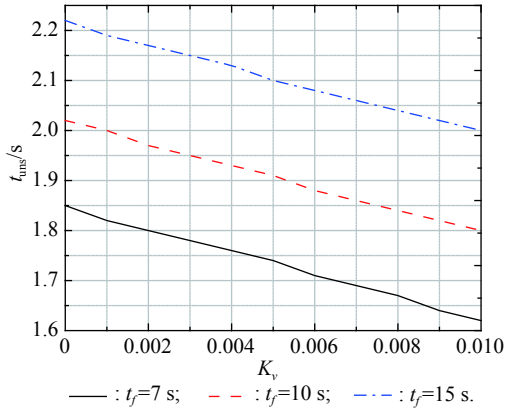

Fig. 19 Relationship between the unstable interval and K_v (K_r=−0.03)

From Fig. 16 and Fig. 17, we know that under the action of the spring torque, the time interval of the unstable state $\bar{t}_{\text{uns}}$ increases with the increase of the torque coefficient. If the final guidance time $\bar{t}_f$ increases, the time interval of unstable state $\bar{t}_{\text{uns}}$ will also increase correspondingly. When K_r is positive, the time interval of unstable state $\bar{t}_{\text{uns}}$ is greater than that when K_r is negative.

From Fig. 18 and Fig. 19, we know that under the action of the damping torque, the time interval of unstable state $\bar{t}_{\text{uns}}$ decreases with the increase of the torque coefficient. If the final guidance time $\bar{t}_f$ increases, the time interval of unstable state $\bar{t}_{\text{uns}}$ will also increase correspondingly. When K_r is positive, the time interval of unstable state $\bar{t}_{\text{uns}}$ is greater than that when K_r is negative.

When the final guidance time $\bar{t}_f$ is a constant, the relationship between the unstable state time interval $\bar{t}_{\text{uns}}$ of the roll-pitch seeker's guidance system and K_r under the action of the spring torque or the damping torque is considered in Fig. 20.

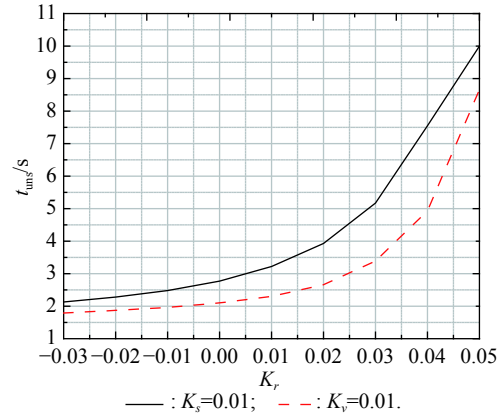

Fig. 20 Relationship between unstable interval and K_r (t_f=10 s)

From Fig. 20, we know that when the final guidance time $\bar{t}_f$ and the torque coefficient are fixed, whether under the action of the spring torque or the damping torque,

the time interval of unstable state $\bar{t}_{\text{uns}}$ will increase with the increase of K_r. When K_r increases from −0.03 to 0.03, the time interval of unstable state $\bar{t}_{\text{uns}}$ increases slowly. When K_r exceeds a certain range, with the increase of K_r, the time interval of unstable state $\bar{t}_{\text{uns}}$ begins to increase rapidly.

$\bar{T}_\alpha$ represents the time constant of the attack angle, which is an important parameter in the DRR parasitic loop of the roll-pitch seeker's guidance system. The DRR parasitic loop parameter $\bar{T}_\alpha$ will also affect the stability of the guidance system. From Fig. 21, we know that under the action of the spring torque, with the increase of $\bar{T}_\alpha$, the suitable spring torque coefficient K_s, which makes the roll-pitch seeker's guidance system critical stable, will decrease first quickly and then slowly. With the increase of K_r, the suitable spring torque coefficient K_s, which makes the roll-pitch seeker's guidance system critical stable, will increase correspondingly. From Fig. 22, we know that under the action of the damping torque, with the increase of $\bar{T}_\alpha$, the suitable damping torque coefficient K_v, which makes the roll-pitch seeker's guidance system critical stable, will decrease first quickly and then slowly. With the change of K_r,K_v changes in a small range.

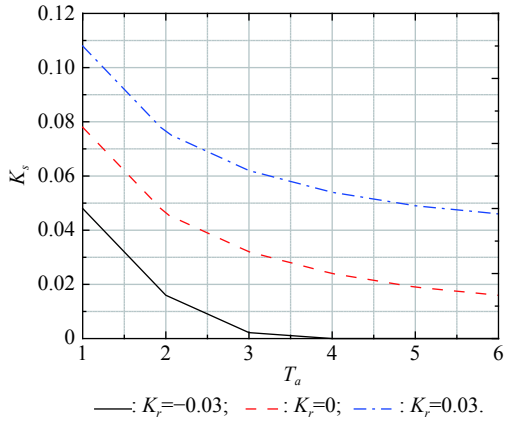

Fig. 21 Relationship between K_s and T_a

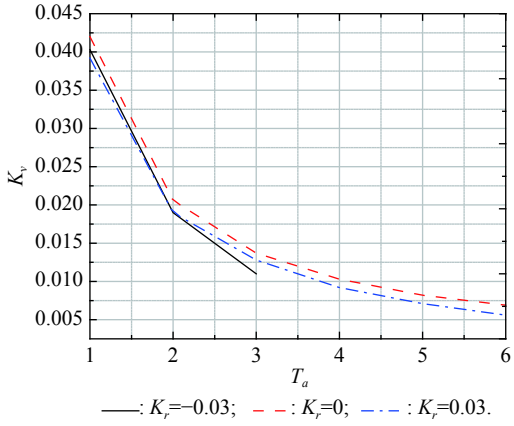

Fig. 22 Relationship between K_v and T_a

5. Simulation analysis of guidance system with roll-pitch seeker

From the analysis in Section 4, we can obtain the following three conclusions:

Conclusion 1 (From Figs. 12−15 and Fig. 20) When K_s(or K_v), $\bar{T}_\alpha$ and $\bar{t}_f$ are the same, the roll-pitch seeker's guidance system is more likely to be in a stable state if K_r is negative. The guidance system will become more instable when K_r increases.

Conclusion 2 (From Figs. 16−19) Under the action of the spring torque, the time interval of unstable state $\bar{t}_{\text{uns}}$ increases with the increase of torque coefficient K_s. Under the action of the damping torque, the time interval of unstable state $\bar{t}_{\text{uns}}$ decreases with the increase of torque coefficient K_v.

Conclusion 3 (From Fig. 21 and Fig. 22) Under the action of the spring torque, with the increase of $\bar{T}_\alpha$, the suitable spring torque coefficient K_s, which makes the roll-pitch seeker's guidance system critical stable, will decrease. Under the action of the damping torque, with the increase of $\bar{T}_\alpha$, the suitable damping torque coefficient K_v, which makes the roll-pitch seeker's guidance system critical stable, will decrease.

These three conclusions are obtained through Lyapunov stability analysis for the guidance system. To show the effectiveness of the stability analysis of the guidance system, we choose suitable parameters combinations for comparison to simulate the model of the complete guidance system.

In Section 2, a complete guidance system model including a roll-pitch seeker is presented. The guidance system guides the missile to fly to the target through the guidance information output by the seeker. Therefore, the accuracy of the guidance information will affect the miss distance of the guidance system. The instability of the roll-pitch seeker will cause errors to the guidance information. Therefore, in the complete guidance system model, the miss distance can be used to evaluate the stability of the guidance system.

We choose the same error interference source as the input of the guidance system and get the dimensionless miss distance of the guidance system under different conditions by simulating different parameter combinations. The guidance system model is shown in Fig. 23. The roll-pitch seeker can only output the LOS angle so that we can choose LOS angle error as the inputs of the guidance system. Simulation conditions and parameter combinations are shown in the following Table 3, in which $N=4$, $V_c=600$ m/s,$V_m=400$ m/s, $t_f=10$ s.

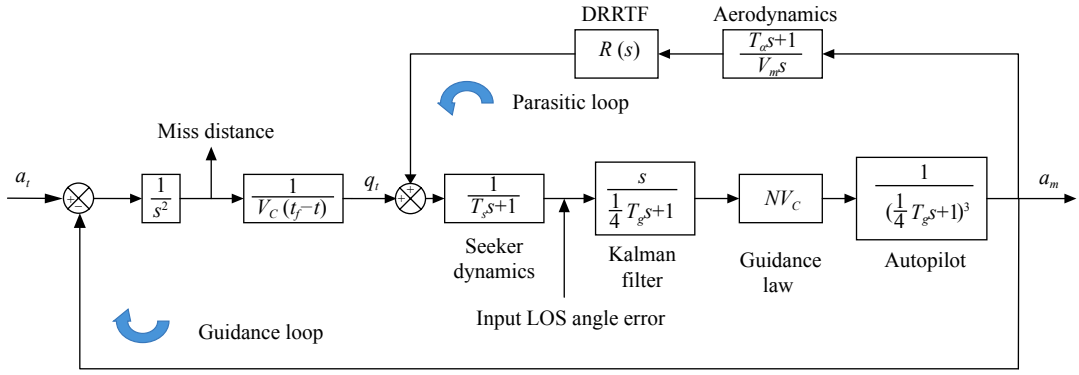

Fig. 23 Guidance system with error inputs

Table 3 Parameters for simulation of guidance system

Figure	Torque	Parameter	Description
Fig. 24	Spring	$\bar{T}_\alpha=3, K_s=0.01,\ K_r\in[-0.03,0.03]$	Verify Conclusion 1: the influence of K_r on the stability of the system
	Damping	$\bar{T}_\alpha=3, K_v=0.01,\ K_r\in[-0.03,0.03]$	
Fig. 25	Spring	$\bar{T}_\alpha=3, K_r=0.03,\ K_s\in[0,0.01]$	Verify Conclusion 2: the influence of K_s on the stability of the system
	Spring	$\bar{T}_\alpha=3, K_r=-0.03,\ K_s\in[0,0.01]$	
Fig. 26	Damping	$\bar{T}_\alpha=3, K_r=0.03,\ K_v\in[0,0.01]$	Verify Conclusion 2: the influence of K_v on the stability of the system
	Damping	$\bar{T}_\alpha=3, K_r=-0.03,\ K_v\in[0,0.01]$	
Fig. 27	Spring	$K_r=0.03, K_s=0.01,\ \bar{T}_\alpha\in[1,6]$	Verify Conclusion 3: the influence of $\bar{T}_\alpha$ on the stability of the system
	Spring	$K_r=-0.03, K_s=0.01,\ \bar{T}_\alpha\in[1,3]$	
Fig. 28	Damping	$K_r=0.03, K_v=0.01,\ \bar{T}_\alpha\in[1,6]$	Verify Conclusion 3: the influence of $\bar{T}_\alpha$ on the stability of the system
	Damping	$K_r=-0.03, K_v=0.01,\ \bar{T}_\alpha\in[1,3]$	

Fig. 24 to Fig. 28 show the simulation results of guidance system's dimensionless miss distance under different parameters conditions. From Fig. 24, we know that when K_s (or K_v), $\bar{T}_\alpha$ and $\bar{t}_f$ are the same, the guidance system will becomes more instable when K_r increases, which can be shown by the increase of dimensionless miss distance in Fig. 24. We can also find that the dimensionless miss distance becomes divergent when $K_r>0.01$ in this simulation. These simulation results can verify Conclusion 1 in Section 4.

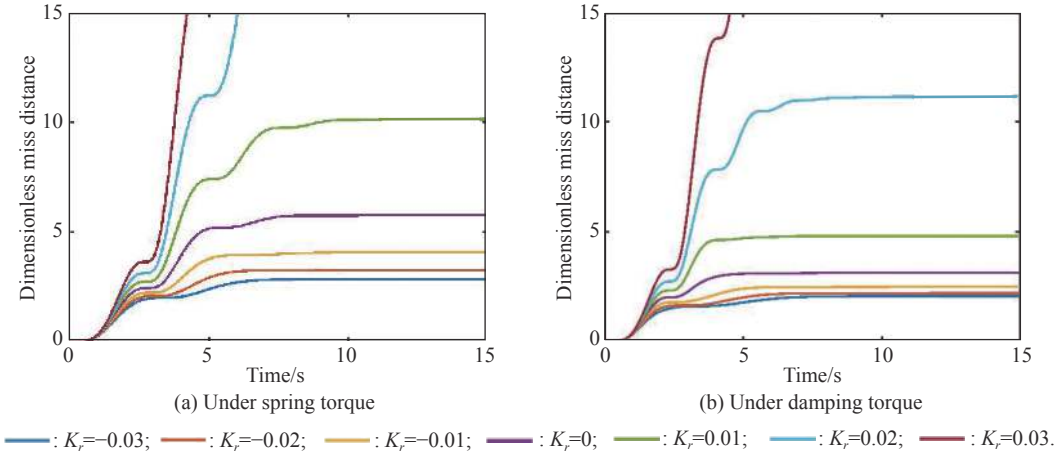

Fig. 24 Dimensionless miss distance with different K_r under spring and damping torques

Fig. 25 and Fig. 26 show the torque coefficients' influence on dimensionless miss distance of the guidance system. In Conclusion 2, $\bar{t}_{\text{uns}}$ represents the time interval of the unstable state. Therefore, the guidance system will be more likely to be stable with the decrease of $\bar{t}_{\text{uns}}$. From Fig. 25 and Fig. 26, we know that under the action of the spring torque, the dimensionless miss distance increases with the increase of K_s and under the action of the damping torque, the dimensionless miss distance decreases with the increase of K_v. From Fig. 25 and Fig. 26, we can

obtain that $\Delta\text{miss} \approx 100\Delta K_s$ when K_r is positive, which means that when K_s increases from 0 to 0.01, the dimensionless miss distance increases by one unit. The dimensionless miss distance with $K_r = -0.03$ is approximately double of that with $K_r = 0.03$. These simulation results can verify Conclusion 2 in Section 4.

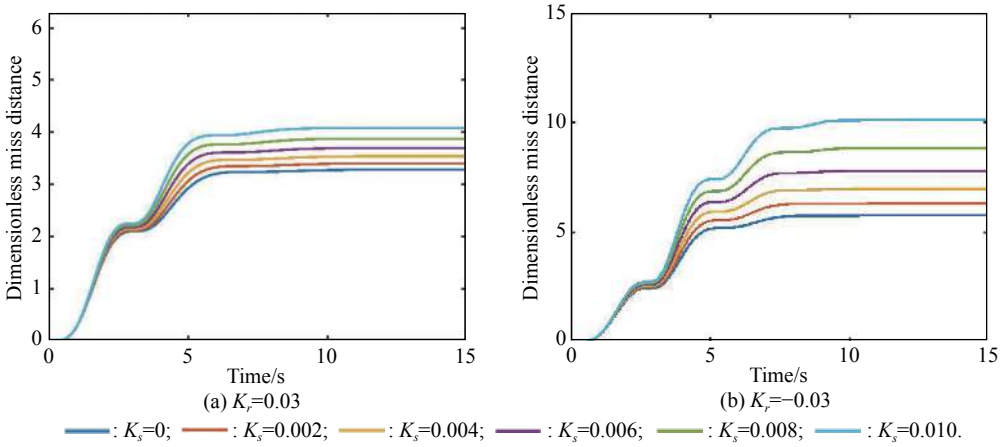

Fig. 25 Dimensionless miss distance with different K_s under spring torque

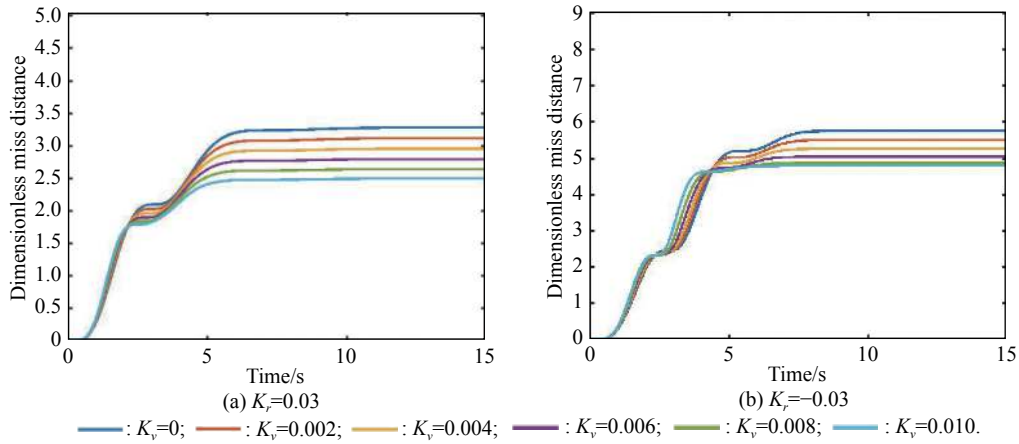

Fig. 26 Dimensionless miss distance with different K_v under damping torque

Fig. 27 and Fig. 28 show that when K_s (or K_v) is the same, the dimensionless miss distance increases with the increase of $\bar{T}_\alpha$, which means the guidance system will become more instable with the increase of $\bar{T}_\alpha$.

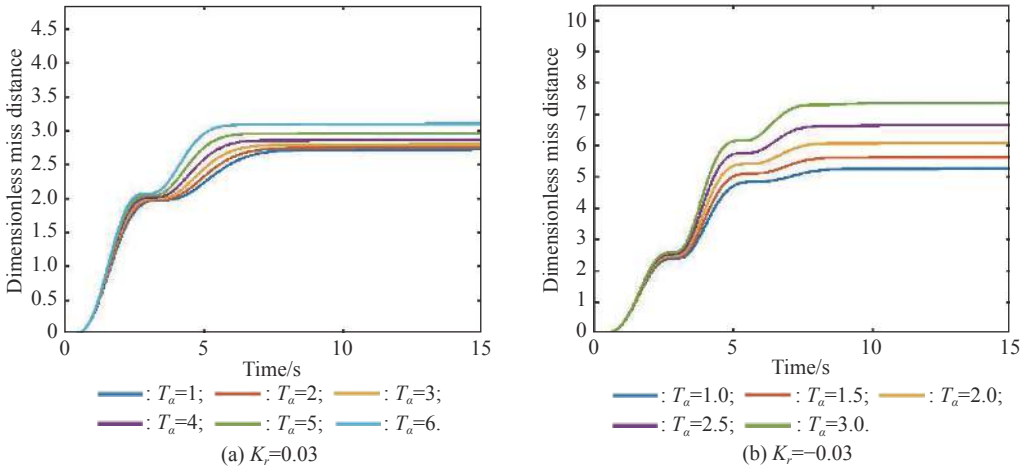

Fig. 27 Dimensionless miss distance with different T_α under damping torque

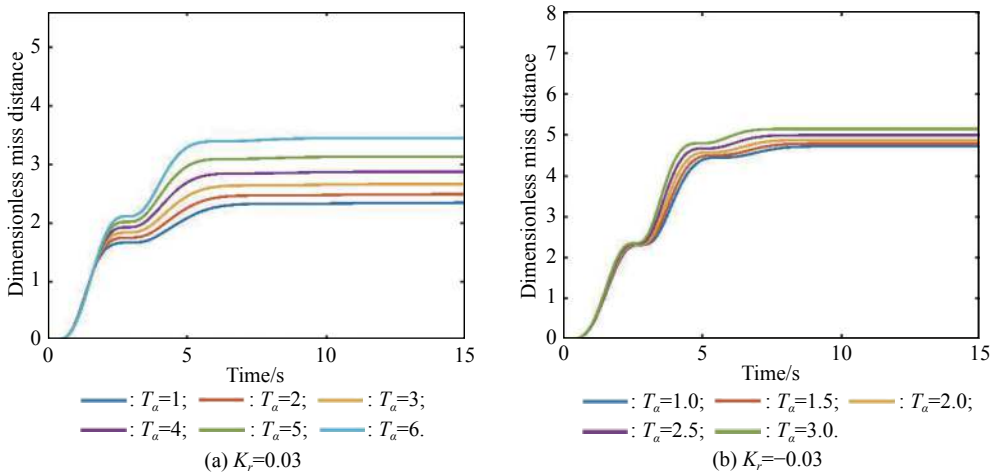

Fig. 28 Dimensionless miss distance with different T_a under damping torque

Under the action of the spring the torque, the dimensionless miss distance with $K_r = -0.03$ is approximately double of that with $K_r = 0.03$. Under the action of the damping torque, the increase of the dimensionless miss distance from $K_r = 0.03$ to $K_r = -0.03$ is not as large as the condition under the spring torque. These simulation results can verify Conclusion 3 in Section 4.

6. Conclusions

In this paper, the DRR and the parasitic loop model of the roll-pitch seeker are established. Based on the Lyapunov stability criterion and the passivity theorem, the relationship between the stability of the guidance system and the parameters of DRR and DRR parasitic loop is simulated and analyzed. From the simulation and analysis, we can draw conclusions as follows:

The stability of the roll-pitch seeker's guidance system is affected by the DRR and the DRR parasitic loop of the roll-pitch seeker. The DRRTF and the model of the DRR parasitic loop is different under the action of different types of disturbance torque. The causes of the roll-pitch seeker's DRR are analyzed systematically, and the relationship between DRR caused by scale deviation and LOS angle is derived for the first time. As a nonlinear time-varying system, roll-pitch seeker's guidance system requires the Lyapunov stability criterion for the stability analysis. By dimensionless variation, the roll-pitch seeker's guidance system can be equivalently simplified, and then Lyapunov stability analysis can be carried out by applying the passivity theorem.

According to the Nyquist analysis, we know that the DRR and DRR parasitic loop parameters $\bar{T}_\alpha, \bar{t}_f, K_s, K_v, K_r$ will affect the stability domain range of the roll-pitch seeker's guidance system. From simulation of the guidance system, we know that when K_s (or K_v), $\bar{T}_\alpha$ and $\bar{t}_f$ are the same, the guidance system will become more instable when K_r increases. The dimensionless miss distance becomes divergent when $K_r > 0.01$ in this simulation.

Under the action of the spring torque, the dimensionless miss distance increases with the increase of K_s and under the action of the damping torque, the dimensionless miss distance decreases with the increase of K_v. We can obtain that $\Delta\text{miss} \approx 100\Delta K_s$ when K_r is positive, which means that when K_s increases from 0 to 0.01, the dimensionless miss distance increases by one unit. The dimensionless miss distance with $K_r = -0.03$ is approximately double of that with $K_r = 0.03$.

When K_s (or K_v) is the same, the dimensionless miss distance increases with the increase of $\bar{T}_\alpha$, which means the guidance system will become more instable with the increase of $\bar{T}_\alpha$. Under the action of the spring torque, the dimensionless miss distance with $K_r = -0.03$ is approximately double of that with $K_r = 0.03$. Under the action of the damping torque, the increase of the dimensionless miss distance from $K_r = 0.03$ to $K_r = -0.03$ is not as large as the condition under the spring torque.

The results of this paper can provide a reference for the stability design and analysis of air-to-air missile with a roll-pitch seeker. At the same time, this paper can also provide a theoretical basis for the design and analysis of DRR and DRR parasitic loop parameters of the roll-pitch seeker and provide a reference for stability analysis of other types of seeker's guidance systems.

References

[1] GUO Y, GUO J H, LIU X, et al. Finite-time blended control for air-to-air missile with lateral thrusters and aerodynamic surfaces. Aerospace Science and Technology, 2020, 97: 105638.

[2] HUI Y L, NAN Y, CHEN S D, et al. Dynamic attack zone of air-to-air missile after being launched in random wind field. Chinese Journal of Aeronautics, 2015, 28(5): 1519–1528.

[3] LIU H Q, YU L, RUAN C W, et al. Tracking air-to-air missile using proportional navigation model with genetic algorithm particle filter. Mathematical Problems in Engineer-

ing, 2016.
[4] MORTAZAVI M R, ALMASGANJ F. Optimal midcourse guidance of an air-to-air missile via SVM and RVM. Soft Computing, 2019, 23(15): 6603–6616.
[5] LI S Y, YANG K, MA J, et al. Anti-interference recognition method of aerial infrared targets based on the Bayesian network. Journal of Optics, 2021, 50(2): 264–277.
[6] LEONID A B, SERGEY A L, VLADLENA V O. Air-to-air missile guidance For nonmaneuverable target interception at maximum distance. TsAGI Science Journal, 2019, 49(7): 753–770.
[7] DONG Z W, GAO F, SUN L, et al. Research on fault intelligent reasoning and diagnosis of air-to-air missile weapon system of a certain armed helicopter. Proc. of the 11th International Conference on Machine Learning and Computing 2019: 147−150.
[8] LI J Q, LI J, QIN L, et al. Optimal design and analysis on high overload buffer structure of passive semi-strapdown inertial navigation system. Sensors, 2020.
[9] JING Z Y, ZHENG T, LI J, et al. Optimized design of an anti-rotation and anti-overload structure based on missile-borne semi-strap-down inertial navigation system. IEEE Access, 2019, 7: 179646–179657.
[10] LIU F, WANG H, AUBRY R. The effects of matched filter on stable performance of semistrapdown inertially stabilized platform. Mathematical Problems in Engineering, 2016. DOI: 10.1155/2016/8389350.
[11] ZHOU X Y, JIA Y, ZHAO Q, et al. Experimental validation of a compound control scheme for a two-axis inertially stabilized platform with multi-sensors in an unmanned helicopter-based airborne power line inspection system. Sensors, 2016, 16(3): 366.
[12] XIE C J, WANG Z Q, WANG R, et al. Feed forward compensation control of dual-axis photoelectric stabilized platform. Journal of Coastal Research, 2015, 2015(73): 771–775.
[13] ZHANG M Y, GUAN Y L, ZHAO W W. Adaptive super-twisting sliding mode control for stabilization platform of laser seeker based on extended state observer. Optik-International Journal for Light and Electron Optics, 2019, 199: 163337.
[14] FU C Y, TIAN Y T, HUANG H Y, et al. Finite-time trajectory tracking control for a 12-rotor unmanned aerial vehicle with input saturation. ISA Transactions, 2018, 81: 52–62.
[15] PUNEET M, VINEET K, RANA K P. A fractional order fuzzy PID controller for binary distillation column control. Expert Systems with Applications, 2015, 42(22): 8533–8549.
[16] ZHANG M Y, LIU H, ZHANG H W, et al. A hybrid control strategy for the optoelectronic stabilized platform of a seeker. Optik-International Journal for Light and Electron Optics, 2019, 181: 1000–1012.
[17] ZHENG D, LIN D F, XU X H, et al. Dynamic stability of rolling missile with proportional navigation & PI autopilot considering parasitic radome loop. Aerospace Science and Technology, 2017, 67: 41–48.
[18] LIN S Y, WANG W, LIN W, et al. The research of loop-shaping method to mitigate the total error effect in air-to-air missiles. Optik-International Journal for Light and Electron Optics, 2019, 181: 923–932.
[19] TIAN S, LIN D F, WANG J, et al. Dynamic stability of rolling missiles with angle-of-attack feedback three-loop autopilot considering parasitic effect. Aerospace Science and Technology, 2017, 71: 592–602.
[20] LI W, WEN Q Q, YANG Y. Stability analysis of spinning missiles induced by seeker disturbance rejection rate parasitical loop. Aerospace Science and Technology, 2019, 90: 194–208.
[21] LIU S X, DU X, XIA Q L. An on-line compensation method for the disturbance rejection rate of seekers. Optik-International Journal for Light and Electron Optics, 2018, 157: 1306–1318.
[22] DU X, LV R, TU H F, et al. The research on infrared seeker with disturbance rejection effect parasitic. Optik-International Journal for Light and Electron Optics, 2018, 170: 409–419.
[23] LIU S X, LU T Y, SHANG T, et al. Dynamic modeling and coupling characteristic analysis of two-axis rate gyro seeker. International Journal of Aerospace Engineering, 2018. DOI: 10.1155/2018/8513684.
[24] CHEN K W, XIA Q L, DU X, et al. Influence of seeker disturbance rejection and Radome error on the Lyapunov stability of guidance systems. Mathematical Problems in Engineering, 2018.
[25] HE F X, DAI L, CHEN Q S, et al. Three-dimensional stability analysis of robotic machining process. Industrial Robot: An International Journal, 2020, 47(1): 82–89.
[26] TOCINO A, SENOSIAIN M. MS-stability of nonnormal stochastic differential systems. Journal of Computational and Applied Mathematics, 2020, 379: 112950.
[27] BAI R, XIA Q L, DU X. The study of guidance performance of a phased array seeker with platform. Optik-International Journal for Light and Electron Optics, 2017, 132: 9–23.
[28] LI X D, YANG X Y. Lyapunov stability analysis for nonlinear systems with state-dependent state delay. Automatica, 2020, 112: 108674.
[29] JOSINEY A S, LUANA H T. Lyapunov stability for impulsive control affine systems. Journal of Differential Equations, 2018.
[30] LIU X, MO B, LIU F X. Line-of-sight stabilization of roll-pitch seeker using differentiator-based disturbance compensation control. Proceedings of the Institution of Mechanical Engineers, Part G: Journal of Aerospace Engineering, 2020, 234(7): 1326–1339.
[31] WANG X C, MO B, LI X, et al. Predictive functional control-based zenith pass controller design for roll-pitch seeker. International Journal of Aerospace Engineering, 2020. DOI: 10.1155/2020/9709341.
[32] LIU S X. Application of roll-pitch seeker to air-to-air missile guidance system. Beijing: Beijing Institute of Technology, 2019. (in Chinese)
[33] BAI R. Key technology of roll-pitch seeker and its application to air-to-air missile. Beijing: Beijing Institute of Technology, 2017. (in Chinese)
[34] KHALIL H K. Nonlinear systems (third edition). New Jersey: Prentice-Hall, Inc, 2002.
[35] MARYAM F, SOHEIL G, HEIDAR A T, et al. A novel cooperative teleoperation framework for nonlinear time-delayed single-master/multi-slave system. Robotica, 2019, 38(3): 475–492.

Biographies

LI Yue was born in 1995. He received his B.E. degree from Beijing Institute of Technology in 2016. He is currently a doctoral student in School of Aerospace Engineering, Beijing Institute of Technology. His main research interests include flight vehicle design, guidance and control.
E-mail: liyue627167955@163.com

WEN Xianghua was born in1982. He received his B.E. degree in ammunition control major from Changsha University of Science and Technology in 2006, and Master's degree in control engineering from Beijing University of Aeronautics and Astronautics in 2015. He is a senior engineer working in the No. 5718 Factory of the Chinese People's Liberation Army. His research interests include guidance and control.
E-mail: 495460738@qq.com

LI Wei was born in 1994. He received his B.E. degree from Beijing Institute of Technology in 2015. He is currently a doctoral student in School of Aerospace Engineering, Beijing Institute of Technology. His main research interests include flight vehicle design, guidance and control.
E-mail: lion_lee1994@126.com

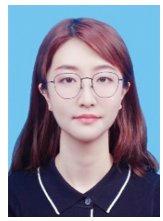

WEI Lan was born in 1994. She received her B.E. degree in electronic information engineering from North University of China in 2017. She is a master in Beijing Institute of Technology. Her research interest is aircraft control.
E-mail: 389968247@qq.com

XIA Qunli was born in 1971. He received his B.E. degree in launcher and design major from Beijing Institute of Technology in 1993, and Master's degree in flight mechanics from Beijing Institute of Technology in 1996. He received his Ph.D. degree in aircraft design from Beijing Institute of Technology in 1999. He is an adjunct professor in Beijing Institute of Technology. His research interests include control and guidance technology.
E-mail: 1010@bit.edu.cn